ARCHIVES OF MECHANICS
Arch. Mech. **72** (4), 355–379, 2020, DOI: 10.24423/aom.3556

Nanofluid flow and heat transfer of carbon nanotube and graphene platelette nanofluids in entrance region of microchannels

M. E. FULLER[1)], J. T. C. LIU[2)]

[1)] *Physico-Chemical Fundamentals of Combustion, RWTH Aachen University, 52062 Aachen, Germany, e-mail: fuller@pcfc.rwth-aachen.de (corresponding author)*

[2)] *School of Engineering, Brown University, Providence, RI 02912, U.S.A., e-mail: joseph_liu@brown.edu*

Suspensions of nano-scale particles in liquids, dubbed nanofluids, are of great interest for heat transfer applications. Nanofluids potentially offer superior thermal conductivity to alternative, pure fluids and are of particular interest in applications where active cooling of power-dense systems is required. In this work, the thermophysical properties of carbon nanotube nanofluids (CNTNf) and those of graphene nanoplatelette nanofluids (GNPNf) as functions of particle volume fraction are deduced from published experiments. These properties are applied to a perturbative boundary layer model to examine how the velocity and temperature profiles (and correspondingly shear stress and surface heat transfer) vary with the nanoparticle concentration in the entrance region of microchannels. Findings of this modeling effort indicate that both shear stress and heat transfer in GNPNf increase with increasing particle concentration. The normalized increase in shear stress is approximately twice that for heat transfer as a function of the GNP particle concentration. Interestingly, CNTNf shows anti-enhancement heat transfer behaviour; an increasing concentration of CNT nanoparticles is associated with both an increase in shear stress and a decrease in the surface heat transfer rate.

Key words: nanofluids, heat transfer, carbon nanotubes, graphene nanoplatelettes.

1. Introduction

Since the pioneering work of Choi and Eastman [1], nanofluids have become widespread in applications and stimulated much work on their fundamental understanding, e.g. [2–10]. Our previous theoretical-numerical work [11–13] performed studies of nanofluids with dispersed spherical metallic nanoparticles (alumina and gold) using a perturbation method for small volume concentration. More recently, carbon nanotubes (CNT) and graphene nanoplatelettes (GNP) have become subjects of intense studies because of their thermophysical properties, e.g. [14–32].

This paper applies the methodologies previously developed by the authors to nanofluids consisting of multi-walled CNT (MWCNT) and GNP dispersed in liquid; we refer to these nanofluid mixtures, respectively, as CNTNf and GNPNf. Both CNT and GNP are graphene structures, based on two-dimensional arrays of carbon atoms. CNT are hollow cylinders where the graphene sheet is "rolled up" either with the edges joined to form a continuous cylinder (and therefore single-atom thick wall, "single-walled", SWCNT) or in a spiral, "scroll" structure [33, 34]. The term MWCNT refers to both multiple concentric single-walled tubes and "scroll" spiral-form tubes where the sheet is wound such that it overlaps itself. GNP, in contrast, consists of stacked or layered sheets of graphene where the layers are held together with van der Waals forces [35]. The thermophysical properties of the nanofluids that are required for this model and analysis are drawn from [14] and [36], respectively. Application to the entrance region of microchannels is made, as measurements in alumina nanofluids indicate that the largest nanofluid effect is in this region [37]. In the entrance region of the channels, the boundary layer thickness is small compared to the tube diameter and simplified modeling may be accomplished by considering the models of boundary layers in flow over flat plates. Both momentum and thermal boundary layers for flow over flat plates are solved problems in laminar flow owing to the respective works of Blasius [38] and Pohlhausen [39].

A thorough overview of recent developments in the use of carbon-based nanofluids for heat transfer and in heat exchangers has beem provided in [27]. Experimental determination of the properties of nanofluid mixtures (discussed in greater detail in Section 2) alone has been the subject of multiple articles. While the totality of articles is too numerous to mention, certain studies are worth recounting. Measurements of thermal conductivity of water-CNT nanofluids [40] show variable enhancement depending on the exact morphology of the CNT utilized, comparing SWCNT of small aspect ratios ("short"), large aspect ratios ("long"), and MWCNT. In the study of [40], the most enhancement is observed for the long SWCNT and the least with MWCNT. The summary in [27] also indicates that there have been multiple reports of viscosity of MWCNT-water nanofluids decreasing relative to the base fluid at low particle loadings (up to 0.2 vol%) and increasing thereafter [41, 42, 43]. For GNP, both viscosity and thermal conductivity were examined by Mehrali *et al.* [44] as a function of the specific surface area of the GNP (300, 500, 750 m^2/g). There, both thermal conductivity and viscosity enhancement were shown to correlate with a specific surface area. For both CNTNf and GNPNf, the variations in density and specific heat with a particle loadings do not exhibit any particularly noteworthy behavior with the mixture properties coinciding with volume-averages [27, 45–47].

Recent studies that have specifically focused on theoretical, physics-based models of nanofluids with an eye towards heat transfer share many similarities.

The use of a similarity variable to combine spatial coordinates as in the original work of BLASIUS [38] and the ensuing non-dimensionalized equations describing the boundary layer is a standard mathematical formulation. This is the general outline of the approach taken in this manuscript and its antecedents [11–13]. In our previous and current work, we apply a perturbation analysis in order to determine the thermophysical properties and the boundary layer solutions. In a recent model for hybrid nanofluids containing two different nanoparticle additives [48], the model development proceeds via similarity variable transform and solution of the boundary layer equations, but utilizes explicit models for the calculation of thermophysical properties as functions of particle concentration and solves the governing equations as functions thereof. The approach of [48] thus offers greater control of the input properties, but is significantly more computationally intensive. Other recent models also have examined boundary layer flow, but with added physics. Some examples include explicit treatment of thermophoresis [49–52], magnetohydrodynamics [51–54], flow in porous media [51, 54–56], natural convection (buoyant or gravitational force) [49, 50, 53, 55–57], and extension to three-dimensional boundary layer models [52–58].

1.1. Perturbative description of mixture properties

The model methodology is given in detail in [11] and [12]. The nanofluid is treated as a base fluid, with properties identified by subscript f, to which a quantity of particles, the subscript p, have been added. Analysis follows a continuum description of the resulting mixture, as in [5], except that the thermophoresis effect, which has been found to be relatively unimportant in [5], is not considered.

The local volume fraction of particles within the nanofluid mixture is identified as ϕ. We take $\phi \ll 1$, which is consistent with experimental nanofluid mixtures [59].

For an arbitrary material property of the nanofluid, z, we differentiate the property with respect to the bulk particle concentration, ϕ_∞, about zero concentration and normalize by the base fluid property,

$$z^* = \frac{z}{z_f} = 1 + \phi\left(\frac{dz^*}{d\phi_\infty}\right)_{\phi=0} + \mathcal{O}(\phi_\infty^2). \tag{1.1}$$

To simplify notation, we indicate derivatives of material properties with respect to the bulk particle concentration, $dz^*/d\phi_\infty$, with "prime" notation, e.g.,

$$z^* = 1 + \phi(z^*)'_{\phi=0} + \mathcal{O}(\phi_\infty^2). \tag{1.2}$$

The properties of the nanofluid required for the analysis of fluid flow and heat transfer are: the density, ρ; specific heat capacity, c; viscosity, μ; and thermal

conductivity, k. We assume that particle diffusion in the base fluid is governed by Brownian diffusion [5] and independent of particle concentration, ϕ. The Brownian motion is a random movement of the nanoparticles within the base fluid due to molecular collisions. The binary diffusion constant for the nanoparticles in the base fluid is assigned the variable D with dimensionality of area per time. Calculating D from the Einstein-Stoke's equation,

$$D = \frac{k_B T}{3\pi\mu d_p} \tag{1.3}$$

where k_B is Boltzmann's constant, T is the fluid temperature, and d_p is the particle diameter. For typical conditions, $T \approx 300K$, $D \approx (5 \times 10^{-19}\,\mathrm{m}^3/\mathrm{s})/d_p$.

1.2. Boundary layer velocity, concentration, and temperature profiles

In the entrance region of the microchannels, we draw an analogy to boundary layer flow over a flat plate. Spatial coordinates are defined from the leading edge of the plate. The abscissa has a zero value at the leading edge and increases with distance parallel to the plate's surface. The ordinate is zero at the plate's surface and measures distance perpendicular to the surface. Free stream properties are identified with subscript ∞; values at the wall by 0. Far from the wall are the free-stream flow velocity, U_∞, and fluid temperature, T_∞. Due to the no-slip boundary condition, the velocity at the wall is zero and the velocity grows in magnitude as one moves perpendicular to the wall until reaching the free stream value. Similarly, should the wall temperature differ from that of the flow, as in a heat transfer application, then there will be a temperature difference relative to the free stream which decreases as one moves away from the wall. The height above the wall or plate at which the velocity reaches the free stream value is the momentum boundary layer thickness; the analog for temperature is the thermal boundary layer thickness. A comprehensive treatment of this subject is provided by Schlichting in [60]. A schematic representation of the velocity and temperature profiles above the wall is shown in Fig. 1.

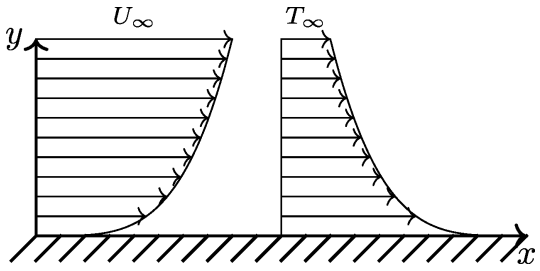

Fig. 1. Schematic representation of velocity and temperature profiles for flow over a plate or wall.

Of ultimate interest is determination of the heat transfer and fluid friction as functions of the nanofluid particle type and concentration relative to the base fluid.

We let u be the fluid velocity parallel to the wall and v is the fluid velocity perpendicular to the wall. The local nanoparticle volume fraction is ϕ and local temperature is T.

Surface heat transfer, q, in the boundary layer is due to the temperature gradient at the wall and enthalpy transport by the nanoparticles, i.e.

$$q_0 = -\left(k\frac{\partial T}{\partial y}\right)_0 + (j_p h_p)_0, \tag{1.4}$$

where the mass flux of particles is j_p, mass per area per time, and the unit enthalpy of the particles, energy per mass, is denoted by h_p.

Utilizing a Fickian diffusion model [61],

$$j_p = -\left(\rho_p D\frac{\partial \phi}{\partial y}\right)_0 + \mathcal{O}(\phi^2). \tag{1.5}$$

Thus, the heat transfer rate is expressed as

$$q_0 = -\left(k\frac{\partial T}{\partial y}\right)_0 - \left(\rho_p D\frac{\partial \phi}{\partial y}h_p\right)_0. \tag{1.6}$$

The surface shear stress, τ_0, force per area, is defined as the product of the fluid viscosity, μ, and the streamwise velocity gradient at the wall, i.e.,

$$\tau_0 = \mu\left(\frac{\partial u}{\partial y}\right)_{y=0}. \tag{1.7}$$

We combine the preceding expressions for heat transfer and mass diffusion with the continuity (Eq. (1.8)), momentum (Eq. (1.9)), energy (Eq. (1.10)), and mass diffusion (Eq. (1.11)) equations for the two-dimensional boundary layer. Momentum is considered in the streamwise direction with a zero pressure gradient. Non-dimensionalization of the equations is performed as in as in [11]. Solution of the continuity, momentum, thermal energy, and mass diffusion equations must be carried out for variable nanofluid properties (as in Eq. (1.2)) for the velocity, particle concentration, and temperature profiles in the steady, two-dimensional boundary layer of laminar flow over a flat plate.

Three dimensionless parameters for the transport in the base fluid are also introduced here: the Prandtl number, Pr, relates viscous to thermal diffusion and is equivalent to $\mu c/k$. The Schmidt number, Sc, relates viscous to mass diffusion and is equivalent to $\mu/\rho D$. The Reynolds number, Re, relates inertia to viscosity and is equivalent to $U_\infty L_c \rho/\mu$ where L_c is a characteristic streamwise length scale

and the free stream velocity, U_∞, is the characteristic velocity associated with this problem.

Spatial coordinates x and y are normalized by L_c to obtain x^* and y^*, respectively. We let u^* be the fluid velocity parallel to the wall normalized by the free stream velocity, U_∞, such that the free stream value is $u^* = 1$. Similarly, v^* is the fluid velocity perpendicular to the wall normalized by the free stream velocity. The local volume fraction is normalized by the bulk concentration, $\Phi = \phi/\phi_\infty$. The temperature field is described non-dimensionally by $\theta = (T - T_\infty)/(T_0 - T_\infty)$.

$$\frac{\partial \rho^* u^*}{\partial x^*} + \frac{\partial \rho^* v^*}{\partial y^*} = 0, \tag{1.8}$$

$$\rho^* \left(u^* \frac{\partial u^*}{\partial x^*} + v^* \frac{\partial u^*}{\partial y^*} \right) = \frac{1}{Re} \frac{\partial}{\partial y^*} \left(\mu^* \frac{\partial u^*}{\partial y^*} \right), \tag{1.9}$$

$$\begin{aligned} \rho^* c^* u^* \frac{\partial \theta}{\partial x^*} + \rho^* c^* v^* \frac{\partial \theta}{\partial y^*} \\ = \frac{1}{Re\, Pr_f} \frac{\partial}{\partial y^*} \left(k^* \frac{\partial \theta}{\partial y^*} \right) + \frac{\phi_\infty}{Re\, Sc_f} \frac{\partial}{\partial y^*} \left(\rho_p^* D^* \frac{\partial \Phi}{\partial y^*} c_p^* \theta \right), \end{aligned} \tag{1.10}$$

$$u^* \frac{\partial \Phi}{\partial x^*} + v^* \frac{\partial \Phi}{\partial y^*} = \frac{1}{Re\, Sc_f} \frac{\partial}{\partial y^*} \left(D^* \frac{\partial \Phi}{\partial y^*} \right). \tag{1.11}$$

The preceding equations are subject to the non-dimensional boundary conditions:

$$\begin{aligned} y^* = 0 : u^* = 0,\ \theta = 1,\ \Phi = \phi_0/\phi_\infty, \\ y^* = \infty : u^* = 1,\ \theta = 0,\ \Phi = 1. \end{aligned}$$

Physically, the boundary conditions have the following meanings: At the plate or wall, $y = y^* = 0$: There, owing to the no-slip boundary condition, the velocity is zero, i.e. $u = u^* = 0$. The temperature at the wall is described by T_0. Normalization of temperature with $\theta = (T - T_\infty)/(T_0 - T_\infty)$ requires $\theta = 1$ at the wall. For Φ, we either define the concentration at the wall (ϕ_0), as is useful in the case of particle removal or injection, or, alternatively, the slope may be defined. In the previous work describing a zero flux wall condition, the boundary condition was specified as $\partial\phi/\partial y^* = 0$ at $y^* = 0$ [11]. The value ϕ_0 is the value of ϕ at the wall, i.e. at $y^* = 0$, and is specified as part of the problem description.

Later, we examine the three cases of $\phi_0 = \phi_\infty$, a uniform particle distribution, $\phi_0 = 0$, in which particles are removed at the wall, and $\phi_0 = 2\phi_\infty$, in which particles are injected at the wall. The three cases correspond to specifying values at the wall of $\Phi = 1$, $\Phi = 0$, and $\Phi = 2$, respectively.

At infinite distance from the plate or wall, $y = y^* = \infty$: the streamwise velocity is at its maximum value, the freestream velocity, $u = U_\infty$, $u^* = 1$. The fluid temperature in the freestream is T_∞; the definition of θ fixes this condition

as $\theta = 0$. Finally, the normalized particle concentration in the freestream must also be unity by definition as Φ is the ratio of the local concentration, ϕ to the freestream concentration ϕ_∞.

By the perturbative expansion, our variables take the form

$$G = G_0 + \phi_\infty G_1 + \mathcal{O}(\phi_\infty^2), \tag{1.12}$$

where G is any one of f (introduced below), u^*, v^*, Φ, or θ.

Spatial coordinates x^* and y^* are recast into the Blasius similarity variable $\eta = y^*\sqrt{Re/x^*}$ and stream function $\psi^* = f(\eta)\sqrt{x^*/Re}$, velocities u^* and v^* become encoded in a single function, f, where $u^* = df/d\eta$ and $v^* = [(\eta(df/d\eta) - f)/(2\sqrt{x^*Re})]$ [38, 60]. The non-dimensional form of the Blasius similarity variable utilized here is obtained by substituting the characteristic length scale L_c into the dimensional form $\eta = y\sqrt{U_\infty/(\nu x)}$, where ν is equivalent to μ/ρ. We need only make the substitutions $x = x^*L_c$ and $y = y^*L_c$ and utilize the aforementioned definition of the Reynolds number, $Re = U_\infty L_c\rho/\mu$.

With our variables perturbative form, following Eq. (1.12), we arrive at a set of differential equations and boundary conditions to characterize our system. Derivatives of f, Φ, and θ are identified with "prime" notation where derivatives are taken with respect to the similarity variable, η. The problems for f_0 and θ_0 ($\phi_\infty = 0$) are well-known from the work of BLASIUS [38] and POHLHAUSEN [39], respectively. Detailed treatments of both problems are compiled in [60].

The solutions to the Blasius momentum boundary layer $[f_0'(\eta)]$ and Pohlhausen thermal boundary layer $[\theta_0(\eta, Pr_f)]$ are depicted in Fig. 2.

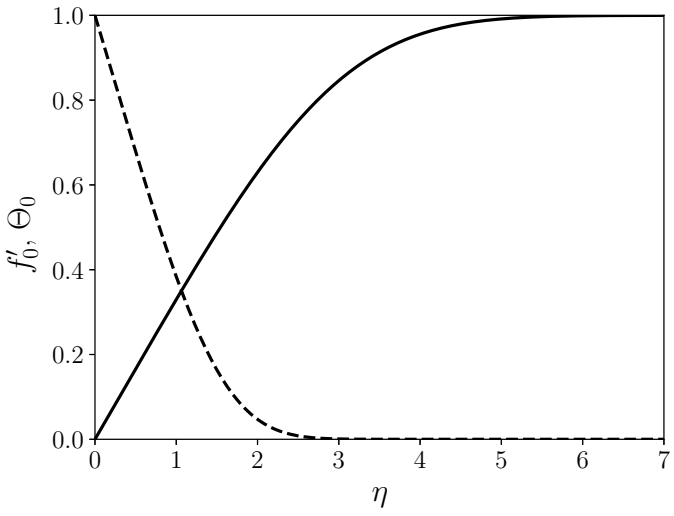

FIG. 2. The zeroth-order solutions to the momentum ($f_0'(\eta)$) and thermal boundary layers ($\theta_0(\eta, Pr_f)$) for the base fluid with $Pr_f = 7.0$. $f_0'(\eta)$: ——; $\theta_0(\eta, Pr_f)$: - - -.

The concentration problem for Φ is necessarily a first-order perturbation as particle concentration is absent in the base fluid. The problems for f_1 and θ_1 define the perturbative influence on f_0 and θ_0 via the freestream particle concentration ϕ_∞ with the functional form given in Eq. (1.12).

Observing the results for the base fluid in Fig. 2, it is possible to observe the boundary layer thickness in the absence of nanoparticles. The function f_0', equivalent to u_0^*, asymptotes by $\eta \gtrsim 5$ and the thermal boundary layer is somewhat thinner as θ_0 asymptotes by $\eta \lesssim 3$.

$$f_1''' + \frac{(f_0 f_1'' + f_0'' f_1)}{2} = \frac{f_0 f_0'' \Phi_1}{2}[(\mu^*)'_{\phi=0} - (\rho^*)'_{\phi=0}] + f_0'' \Phi_1' (\mu^*)'_{\phi=0}, \tag{1.13}$$

$$f_1(0) = f_1'(0) = f_1(\infty) = 0,$$

$$\theta_1'' + \frac{Pr_f(f_0\theta_1' + f_1\theta_0')}{2} = -\theta_0''\Phi_1[(k^*)'_{\phi=0} - (\rho^* c^*)'_{\phi=0}] - \theta_0'\Phi_1'(k^*)'_{\phi=0} - \frac{\rho_p^* c_p^* D^*}{Sc_f}(\Phi_1'\theta_0)', \tag{1.14}$$

$$\theta_1(0) = \theta_1(\infty) = 0,$$

$$\Phi_1'' + \frac{Sc_f f_0 \Phi_1'}{2} = 0, \tag{1.15}$$

$$\Phi_1(0) = \Phi_0, \quad \Phi_1(\infty) = 1.$$

The resulting fundamental equations resemble those of the compressible boundary layer because of the dependence of flow quantities on the volume fraction, which is determined by its diffusion equation [11, 12]. It is worth observing that assuming the same binary diffusion constant and particle diameter across nanofluids, the solution to Eq. (1.15) will be identical and independent of the particle properties discussed below and recorded in Table 1.

2. Particle and nanofluid properties

To examine and predict the properties of CNTNf and GNPNf, material properties of representative nanofluids were either taken directly from experimental observations ("exp") [14, 36] or approximated from the properties of the nanoparticles via mixture theory ("mix") [11]. In the case of experimental measurements, density, heat capacity, thermal conductivity, or viscosity of a prepared nanofluid is measured. Mixture theory estimates the nanofluid properties by a volume-weighted average of the property of interest for the base fluid and for the nanoparticle. The CNTNf values reported by [14] are for multi-walled CNT (MWCNT) particles in water at 1% volume concentration. The experimental values of [14] are used as they represent a complete set of properties for a particular CNTNf

preparation rather than pick individual properties from varying sources. Comparing the values of [14] with others reported in literature, there is a strongly non-linear effect reported for the effect on thermal conductivity: if the real effect of nanoparticle addition to the base fluid on a property of interest is (strongly) non-linear, then this modeling approach is not strictly valid. However, based on the history of perturbation analysis and linearization via Taylor series expansion, by appropriately bounding the maximum nanoparticle concentration, it should be possible to define a region in which the model can offer useful predictions. Examination of the modeling results with the goal of determining the conditions for which the model is valid is discussed in greater detail, below, in Section 3.4.

The value utilized in this work is $(k^*)'_{\phi=0} = 2.5$ taken from data at 1% volume particle concentration. Recent work [40] on experimental measurements of MWCNT-water nanofluids shows a wide range of possible values of $(k^*)'_{\phi=0}$ (as defined via Eq. (1.2)) ranging from approximately $(k^*)'_{\phi=0} \approx 7$ at $\phi = 0.0048$ up to $(k^*)'_{\phi=0} \approx 45$ at $\phi = 0.0005$. The lower value at higher concentration is consistent with earlier findings ($(k^*)'_{\phi=0} \approx 8$ at $\phi = 0.006$ [22]) and the higher value at lower concentration is trend-wise consistent with other experiments as well ($(k^*)'_{\phi=0} \approx 60$ at $\phi = 0.001$ [62]).

Similarly, for the relationship of nanofluid viscosity to nanoparticle concentration for MWCNT-water mixtures, there are experimental data in literature which suggest non-linear behaviour in the very low particle-loading conditions. Data recently presented in [32] show that for $\phi \lesssim 0.001$ the nominal value of $(\mu^*)'_{\phi=0} \approx 200$, which agrees with the values reported by [14] and utilized in this work. For particle loadings an order of magnitude lower, however, [32] reports data which suggest $(\mu^*)'_{\phi=0} \gtrsim 500$.

The GNPNf values for $(\mu^*)'_{\phi=0}$ and $(k^*)'_{\phi=0}$ as reported by [36] are consistent with results of other experiments, such as those of [44] and reported in recent reviews [27]. The non-dimensionalized values describing the thermophysical properties of the nanofluids as a function of particle concentration are summarized in Table 1.

Table 1. Nanoparticle effects on nanofluid properties.

	CNTNf [14]	GNPNf [36]
$(\rho^*)'_{\phi=0}$	0.4 (exp)	1.3 (mix)
$(\rho^* c^*)'_{\phi=0}$	−1.62 (exp)	−0.62 (mix)
$(\mu^*)'_{\phi=0}$	200 (exp)	350 (exp)
$(k^*)'_{\phi=0}$	2.5 (exp)	210 (exp)
$(\mu^*)'_{\phi=0} - (\rho^*)'_{\phi=0}$	199.6	348.7
$(k^*)'_{\phi=0} - (\rho^* c^*)'_{\phi=0}$	4.12	210.62

3. Discussion and results

The numerical solution of the governing equations was accomplished by sequentially solving for f_0, f_1, Φ_1, θ_0, and θ_1. Unknown boundary conditions at the wall were iteratively determined by casting method and the differential equations were solved utilizing the LSODE routine [63] as implemented in Octave [64].

Nanoparticle effects are not limited to augmenting the molecular transport coefficients. In convective flows, both the perturbation temperature and velocity (and concentration) profiles are altered owing to convective transport effects. The net effect in the perturbation problem is revealed by the competition between molecular transport and convective transport, represented by the last two rows in Table 1, $(\mu^*)'_{\phi=0} - (\rho^*)'_{\phi=0}$ and $(k^*)'_{\phi=0} - (\rho^* c^*)'_{\phi=0}$. The convective effects are also interpreted as inertia effects as they are reflected by the rate of change or adjustment process to be balanced by molecular transport.

Examining the governing equations derived for velocity, particle concentration, and temperature, some observations can be made about the behavior of the nanofluid in comparison with the base fluid. Examining Eq. (1.13), the nanofluid effects appear on the right side in the term $[(\mu^*)'_{\phi=0} - (\rho^*)'_{\phi=0}]$. For the temperature profile, Eq. (1.14), the direct nanofluid effects appear on the right side; the inhomogeneous, convective effect of $\frac{1}{2}\theta'_0 f_1 Pr_f$ is indirect.

The numerical solution of the various cases utilizes water as the base fluid, for which $\nu = \mu/\rho \approx 1 \times 10^{-6}\,\mathrm{m}^2/\mathrm{s}$. As in [12], the Schmidt number is taken as 2×10^4, corresponding to a nanoparticle diameter $\mathcal{O}(10\text{ nm})$.

The CNT particles are given as having diameters between 20 and 30 nm and lengths (thickness) between 1 and 5 nm [14] . The GNP of are similarly described as having a thickness of 1 to 5 nm [36].

3.1. Solid wall (zero particle flux)

The volume concentration, for a solid wall, has a zero flux wall boundary condition ($\Phi'_1(0) = 0 \leftrightarrow \Phi_0 = 1$). In the absence of sources (or sinks), it thus remains constant at the free stream value [11, 12]. Expressed in terms of solution to Eq. (1.15), $\Phi_1 = 1\,\forall\eta$.

The profiles f'_1, θ_1 (and $(\Phi_1 = 1)\forall\,\eta$) for CNTNf and GNPNf are shown in Figs. 3 and 4.

For both nanofluids, we observe that the function f'_1 reaches its asymptote at $\eta \lesssim 6$, which is greater than the value for f'_0 (Fig. 2). Thus, the perturbative effect is present beyond the boundary layer thickness of the base fluid, leading to an overall thickening of the boundary layer.

Owing to the large viscosity effect relative to inertia for both nanofluids, (Table 1), the factor $(\mu^*)'_{\phi=0} - (\rho^*)'_{\phi=0} > 0$, in which case the velocity profile is

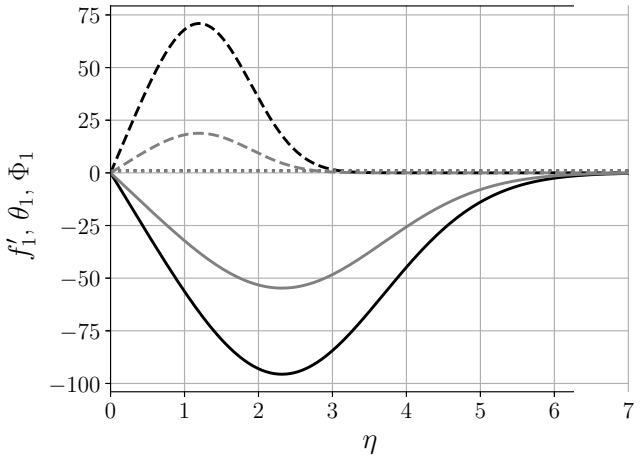

FIG. 3. The first-order perturbation functions with zero particle flux at the wall $(\Phi(0, Sc_f) = 1)$, $Pr_f = 7.0$, $Sc_f = 2 \times 10^4$; $f_1'(\eta)$: GNPNf: ——, CNTNf: ——; $\theta_1(\eta, Pr_f)$: GNPNf: – – –, CNTNf: – – –; $\Phi_1(\eta, Sc_f)$: GNPNf: ·····, CNTNf: ····· (identical solutions $(\Phi_1 = 1)\forall\eta$).

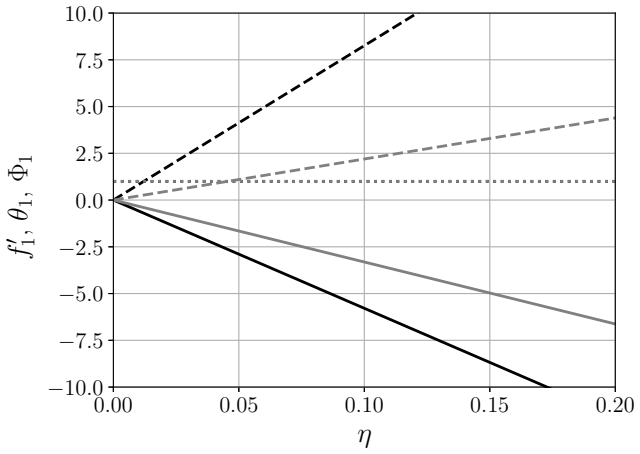

FIG. 4. The first-order perturbation functions with zero particle flux at the wall $(\Phi(0, Sc_f) = 1)$, $Pr_f = 7.0$, $Sc_f = 2 \times 10^4$, detail view. $f_1'(\eta)$: GNPNf: ——, CNTNf: ——; $\theta_1(\eta, Pr_f)$: GNPNf: – – –, CNTNf: – – –; $\Phi_1(\eta, Sc_f)$: GNPNf: ·····, CNTNf: ····· (identical solutions $(\Phi_1 = 1)\forall\eta$).

stretched because of viscous diffusion; as $(f_0' \geq 0)\,\forall\eta$ and $(f_1' \leq 0)\,\forall\eta$, the overall effect is to not only thicken the boundary layer layer, but to reduce the value of $u^* = u_0^* + \phi_\infty u_1^* + \mathcal{O}(\phi_\infty^2)$ throughout the domain.

The magnitude of the effect on the momentum boundary layer and streamwise velocity is more severe for GNPNf, reaching a negative maximum larger than that of the CNTNf because of the stronger viscosity effect. This is in contrast to previous studies [11–13] of alumina and gold nanofluids where

$$(\mu^*)'_{\phi=0} - (\rho^*)'_{\phi=0} < 0.$$

The first-order nanofluid effect on the temperature profile is also shown in Figs. 3 and 4. As with momentum, the GNPNf shows stronger modification of the temperature profile than CNTNf because of the stronger convective transport effect ($(k^*)'_{\phi=0} - (\rho^* c^*)'_{\phi=0}$, Table 1). A visual comparison of Figs. 2 and 3, however, indicates that there is negligible impact on the thermal boundary layer thickness in both nanofluid cases.

In the first-order perturbation theory, the nanofluid effect is defined, and embedded in, the dimensionless slope times the volume fraction. Referring back to [11], in this linear perturbation model, the normalized shear stress, τ^*, and surface heat transfer, q^* reduce to the following:

$$\tau^* = 1 + \phi_\infty[(\mu^*)'_{\phi=0} + f_1''(0)/f_0''(0)] \equiv 1 + \phi_\infty(\tau^*)'_{\phi=0}, \tag{3.1}$$

$$q^* = 1 + \phi_\infty[(k^*)'_{\phi=0} + \theta_1''(0)/\theta_0''(0)] \equiv 1 + \phi_\infty(q^*)'_{\phi=0}. \tag{3.2}$$

The surface heat transfer and shear stress results are then expressed in terms of the slopes: for CNTNf, $(\tau^*)'_{\phi=0} = 100.2$, $(q^*)'_{\phi=0} = -31.54$. For GNPNf, $(\tau^*)'_{\phi=0} = 175.7$, $(q^*)'_{\phi=0} = 82.10$.

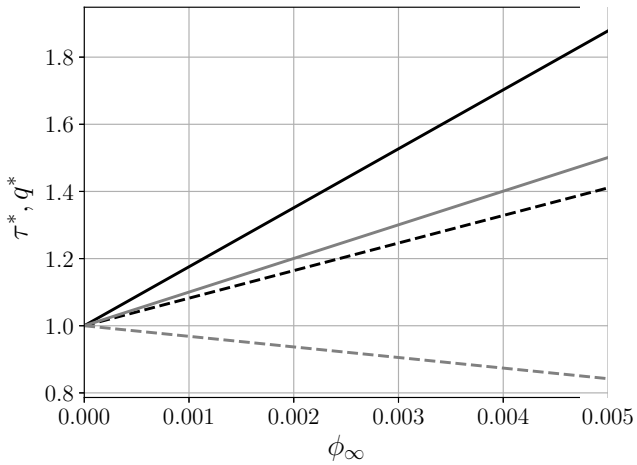

Fig. 5. Heat transfer enhancement and shear stress rise as functions of volume fraction with zero particle flux at the wall ($\Phi(0, Sc_f) = 1$), $Pr_f = 7.0$, $Sc_f = 2 \times 10^4$. τ^*: GNPNf: ——, CNTNf: ——; q^*: GNPNf: – – –, CNTNf: – – –.

As may be observed from the preceding values and in Fig. 5, for both CNTNf and GNPNf, the increase is heat transfer relative to the increase in shear stress is less than unity, i.e. $q^*/\tau^* < 1$. Further, it is noteworthy that $(q^*)'_{\phi=0} < 0$ for CNTNf. In previous studies of alumina and gold nanofluids [11, 12], all the slopes are positive, i.e. such nanofluids increase the surface heat transfer and shear stress to the various degrees dictated by the respective thermophysical properties. It is important to explicitly note that the magnitude of the negative slope will necessarily impose a bound on the applicability of the model: values of $q^* < 0$ or $\tau^* < 0$ are non-physical and accordingly restrict the range in which this model may be valid. Through simple manipulation of Eq. (3.2), it is clear that the material properties of the CNTNf given in Table 1 must be collectively invalid for $\phi_{cr} \gtrsim (-[(q^*)'_{\phi=0}]^{-1}) = 0.0274$ and that linear scaling of the material properties about zero concentration of particles is not representative for CNTNf with particle concentrations in the vicinity of ϕ_{cr}.

There are some data available in the literature with which results may be compared: a study of a CNTNf consisting of MWCNT in water at $\phi \leq 0.01$ found that for fluid flow undergoing transition from laminar to turbulent, "transition flow", at $Re_D = 2000$, $8 \lesssim (q^*)'_{\phi=0} \lesssim 15$ between about 20 and 70 tube diameters [15]. However, the data measured closest to the entrance region, at approximately 10 diameters, showed much less and even negative values, $-5 \lesssim (q^*)'_{\phi=0} \lesssim 3$. GNP were mixed into a hybrid water-ethylene glycol base fluid in [45]. Experimental measures on mixtures with $\phi \leq 0.005$ taken in an automotive radiator showed $50 \lesssim (q^*)'_{\phi=0} \lesssim 300$, which is consistent with the results reported here, but also showed a general trend of the value of $(q^*)'_{\phi=0}$ decreasing with increasing Reynolds number. Also from [45], measured pressure loss suggests $100 \lesssim (\tau^*)'_{\phi=0} \lesssim 800$, trending downward with increasing Reynolds number and showing some dependence on ϕ, with increased particle concentration showing lower pressure loss at the same Reynolds number.

3.2. Porous wall (non-zero particle flux)

It is now worth examining CNTNf and GNPNf in the case of porous walls where the particle concentration may differ from that in the bulk fluid. The case of particle removal, with zero particle concentration at the wall, $\Phi(0, Sc_f) = 0$, is considered first and the perturbation functions are shown in Figs. 6 and 7. It is only on very close examination of Fig. 6 that any difference to Fig. 3 is observable; comparison of Figs. 7 and 4, however, makes clear the impact of the particle concentration on the perturbative functions at the wall. The values of $(\tau^*)'_{\phi=0}$ for both CNTNf and GNPNf decrease and change sign, indicating absolute reduction in the nanofluid shear stress relative to the base fluid and to the solid wall case for low particle loadings. Heat transfer is nearly unchanged

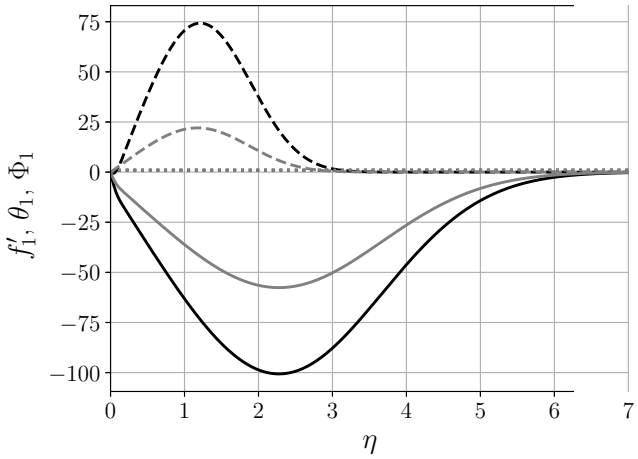

Fig. 6. The first-order perturbation functions with particle removal (zero concentration) at the wall ($\Phi(0, Sc_f) = 0$), $Pr_f = 7.0$, $Sc_f = 2 \times 10^4$. $f_1'(\eta)$: GNPNf: ——, CNTNf: ——; $\theta_1(\eta, Pr_f)$: GNPNf: – – –, CNTNf: – – –; $\Phi_1(\eta, Sc_f)$: GNPNf: ·····, CNTNf: ····· (identical solutions).

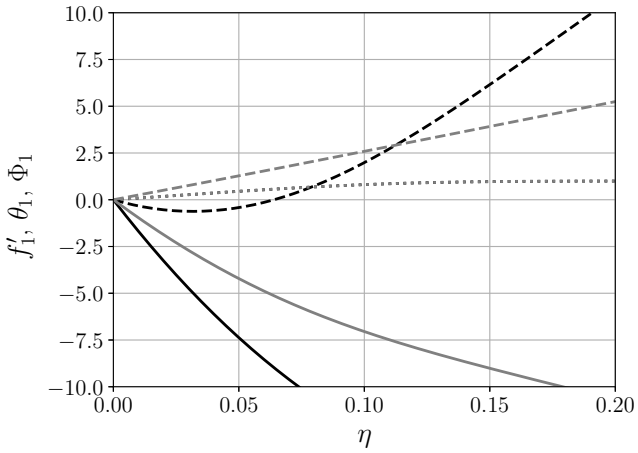

Fig. 7. The first-order perturbation functions with particle removal (zero concentration) at the wall ($\Phi(0, Sc_f) = 0$), $Pr_f = 7.0$, $Sc_f = 2 \times 10^4$, detail view. $f_1'(\eta)$: GNPNf: ——, CNTNf: ——; $\theta_1(\eta, Pr_f)$: GNPNf: – – –, CNTNf: – – –; $\Phi_1(\eta, Sc_f)$: GNPNf: ·····, CNTNf: ····· (identical solutions).

for CNTNf with particle removal at the wall, but is greatly enhanced for GNPNf. The predicted impact on shear stress and heat transfer is shown in Fig. 8. These predictions for the case of particle removal at the wall must be taken with a grain

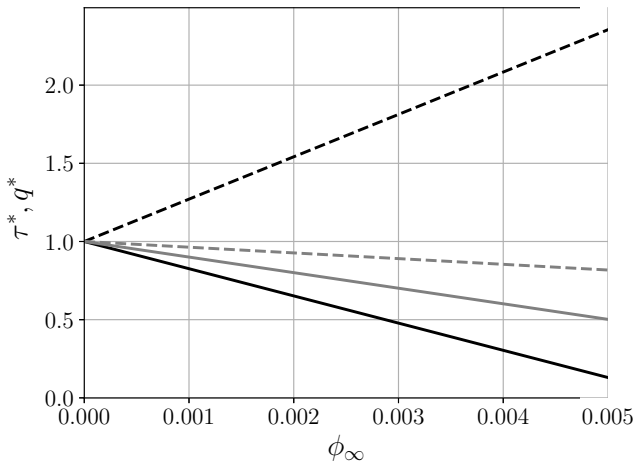

FIG. 8. Heat transfer enhancement and shear stress rise as functions of volume fraction with particle removal (zero concentration) at the wall ($\Phi(0, Sc_f) = 0$), $Pr_f = 7.0$, $Sc_f = 2 \times 10^4$. τ^*: GNPNf: ——, CNTNf: ——; q^*: GNPNf: – – –, CNTNf: – – –.

of salt, however, as the negative values of $(\tau^*)'_{\phi=0}$ lead to values of $\phi_{cr} \lesssim 0.0101$ for CNTNf and $\phi_{cr} \lesssim 0.0058$ for GNPNf.

Turning to particle injection, results are generated for a particle concentration at the wall twice that in the bulk fluid, $\Phi(0, Sc_f) = 2$. The associated

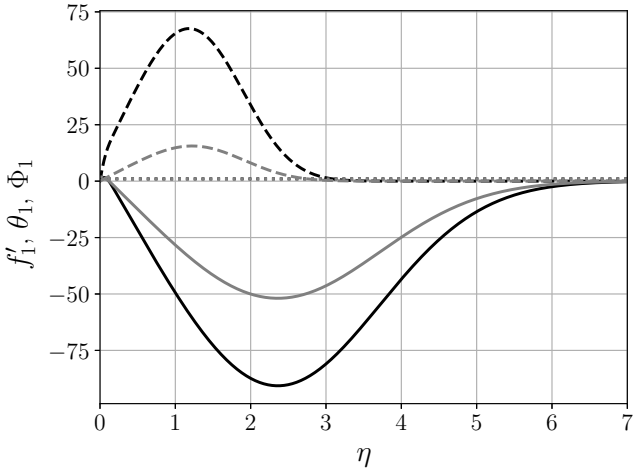

FIG. 9. The first-order perturbation functions with particle injection at the wall ($\Phi(0, Sc_f) = 2$), $Pr_f = 7.0$, $Sc_f = 2 \times 10^4$. $f_1'(\eta)$: GNPNf: ——, CNTNf: ——; $\theta_1(\eta, Pr_f)$: GNPNf: – – –, CNTNf: – – –; $\Phi_1(\eta, Sc_f)$: GNPNf: ·····, CNTNf: ····· (identical solutions).

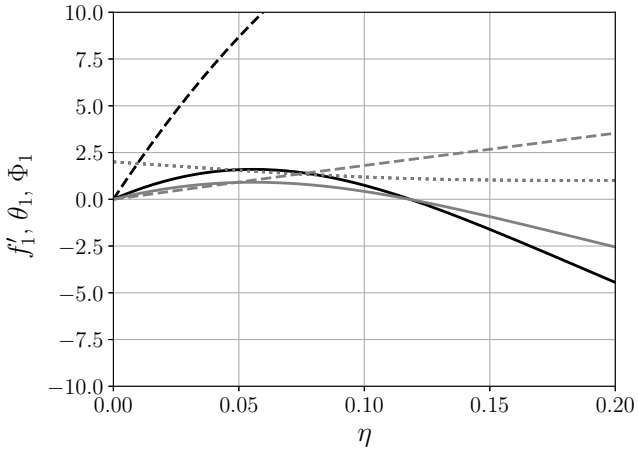

Fig. 10. The first-order perturbation functions with particle injection at the wall ($\Phi(0, Sc_f) = 2$), $Pr_f = 7.0$, $Sc_f = 2 \times 10^4$, detail view. $f_1'(\eta)$: GNPNf: ——, CNTNf: ——; $\theta_1(\eta, Pr_f)$: GNPNf: – – –, CNTNf: – – –; $\Phi_1(\eta, Sc_f)$: GNPNf: ·····, CNTNf: ····· (identical solutions).

perturbation functions are shown in Fig. 9 and in detail in Fig. 10. Here, shear stress increases and heat transfer decreases for both nanofluids relative to the solid wall, with the heat transfer slopes becoming negative, i.e. $(q^*)'_{\phi=0} < 0$, for both fluids. Shear stress and heat transfer as a function of particle loading for the case of wall injection are shown in Fig. 11. The upper restrictions on the

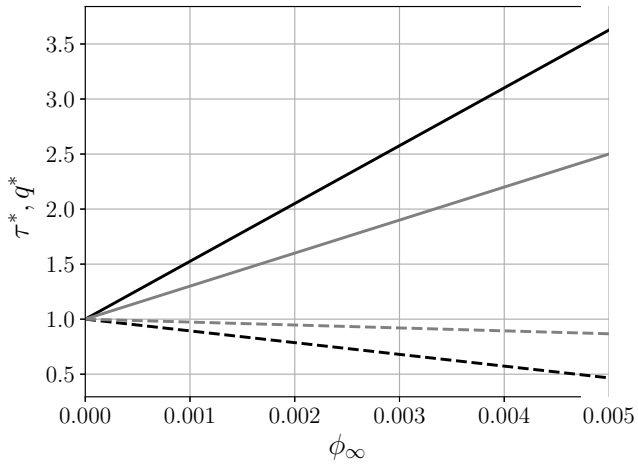

Fig. 11. Heat transfer enhancement and shear stress rise as functions of volume fraction with particle injection at the wall ($\Phi(0, Sc_f) = 2$), $Pr_f = 7.0$, $Sc_f = 2 \times 10^4$. τ^*: GNPNf: ——, CNTNf: ——; q^*: GNPNf: – – –, CNTNf: – – –.

valid range of the model, for this case become $\phi_{cr} \lesssim 0.0377$ for CNTNf and $\phi_{cr} \lesssim 0.0094$ for GNPNf.

The computed values of $(\tau^*)'_{\phi=0}$ and $(q^*)'_{\phi=0}$ for CNTNf and GNPNf for each of the three cases of particle concentration at the wall are provided in Table 2.

Table 2. Nanofluid transport results.

Case	$(\tau^*)'_{\phi=0}$	$(q^*)'_{\phi=0}$
GNPNf, $\Phi(0, Sc_f) = 0$	-174.00	270.90
GNPNf, $\Phi(0, Sc_f) = 1$	175.65	82.10
GNPNf, $\Phi(0, Sc_f) = 2$	525.30	-106.69
CNTNf, $\Phi(0, Sc_f) = 0$	-99.60	-36.50
CNTNf, $\Phi(0, Sc_f) = 1$	100.20	-31.54
CNTNf, $\Phi(0, Sc_f) = 2$	300.00	-26.58

3.3. Comparison with metallic nanofluids

It is worth briefly discussing a comparison of these carbon particle nanofluids, CNTNf and GNPNf, with alumina and gold nanofluids investigated previously with the same modeling approach [11, 12]. As mentioned above, interest in nanofluids is concentrated on applications to improve heat transfer. A nanofluid whose increase in heat transfer is proportionally outstripped by the increase in pumping power, characterized by shear stress, $q^*/\tau^* < 1$, is not going to provide the desired benefit in most cases as heat transfer could be increased at lower cost by increasing the pumping rate, rather than adding nanoparticles.

A general analysis for competition between increased shear stress and increased heat transfer was made in [15] in which it was determined that the requirement for a practical nanofluid, i.e. one in which the benefits outweigh the costs, is $(\mu^*)'_{\phi=0} \leq 4(k^*)'_{\phi=0}$.

Comparisons of CNTNf and GNPNf with the alumina and gold nanoparticle simulations of [11] and [12] for the solid wall and porous walls cases of particle removal and injections are provided, respectively, in Figs. 12, 13, and 14.

Examining the comparisons at each wall condition, it is quite explicit that for the solid wall, Fig. 12, the metallic nanoparticles offer near-unity ratios of heat transfer to shear stress enhancement, with alumina particles out-performing gold and achieving greater gains in heat transfer than in shear stress. The carbon nanofluids show significantly poorer performance and exhibit proportionally larger impacts on the nanofluid properties relative to metallic particles.

Turning to the case of particle removal at the wall, Fig. 13, both carbon nanofluids show a positive, enhancing behavior, but for GNPNf $\phi_{cr} \lesssim 0.0058$. When compared with experimental volume fractions of metallic particles, this

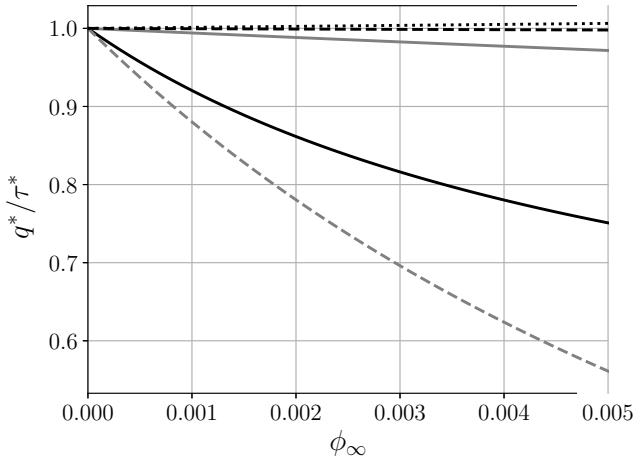

Fig. 12. Heat transfer enhancement and shear stress rise as functions of volume fraction with zero particle flux at the wall ($\Phi(0, Sc_f) = 1$), $Pr_f = 7.0$, $Sc_f = 2 \times 10^4$. GNPNf: ——, CNTNf: – – –, Alumina: ·····, Gold (mix): ——, Gold (MD): – – –.

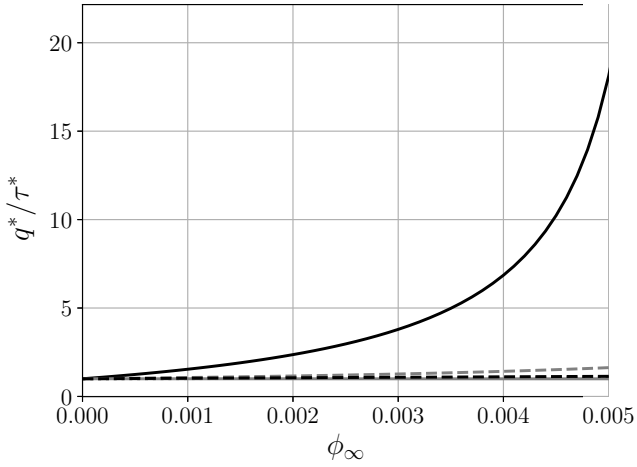

Fig. 13. Heat transfer enhancement and shear stress rise as functions of volume fraction with zero particle concentration at the wall ($\Phi(0, Sc_f) = 0$), $Pr_f = 7.0$, $Sc_f = 2 \times 10^4$. GNPNf: ——, CNTNf: – – –, Alumina: ·····, Gold (mix): ——, Gold (MD): – – –.

is extremely low, cf. [59], but it is seemingly acceptable for the range of volume fractions found in carbon and graphene particle nanofluids, cf. [40].

Finally, in the case of particle injection, Fig. 14, the results are visually similar to the solid wall case. The ratio of heat transfer to shear stress enhancement is less than unity for all materials, but again the metallic nanoparticles and carbon nanoparticles are distinctly separated from each other.

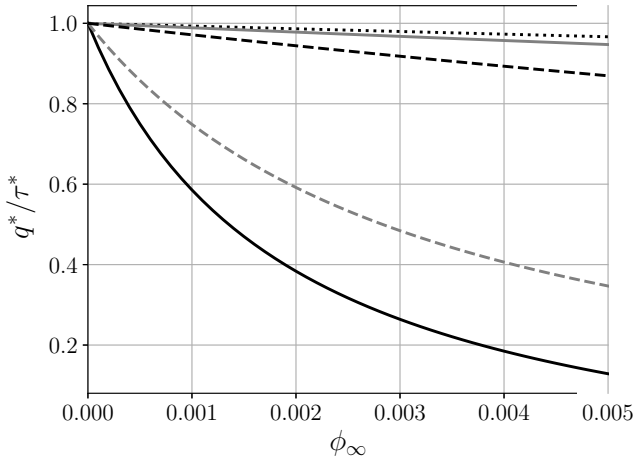

FIG. 14. Heat transfer enhancement and shear stress rise as functions of volume fraction with particle injection at the wall ($\Phi(0, Sc_f) = 2$), $Pr_f = 7.0$, $Sc_f = 2 \times 10^4$. GNPNf: ——, CNTNf: – – –, Alumina: ·····, Gold (mix): ——, Gold (MD): – – –.

3.4. Model limitations

In each of the cases examined, the value of ϕ_{cr} has been determined to identify a loose upper bound on the range for which the model utilized here may be appropriate. The lower values of ϕ_{cr} for GNPNf versus CNTNf are a direct effect of the more dramatic impact on transport in the nanofluid effected by GNP in comparison with CNT. The values of $(\mu^*)'_{\phi=0}$ and $(k^*)'_{\phi=0}$ are both greater for GNPNf than CNTNf, necessarily leading to a breakdown in linearity at lower values of ϕ. It is thus appropriate to also discuss the uncertainty in the value of $(k^*)'_{\phi=0}$ taken for CNTNf. Recalling the reported values in literature, there is a trend of proportionally greater enhancement in thermal conductivity at lower concentrations. Including this trend would have the effect of introducing feedback into our current linearization where as the input value of $(k^*)'_{\phi=0}$ is adjusted up to correspond to an experimental measurement at a lower particle concentration, ϕ, the value of ϕ_{cr} would also fall. The International Nanofluid Property Benchmark Exercise (INPBE) [59] demonstrated good agreement among over thirty research groups in measured thermal conductivity of nanofluids and good agreement to effective medium theory [65] to model the nanofluid thermal conductivity as a function of particle loading. The experimental data measured in [40] and presented in [27] stand in contrast to other publications showing good agreement to approximations per Eq. (1.2) for viscosity and thermal conductivity [66, 15, 45].

4. Conclusion

The present studies indicate that both CNTNf and GNPNf incur very large increases in shear stress at the wall relative to alumina and gold nanofluids; similarly for surface heat transfer for GNPNf but the relative increase is only about half as great as the relative increase in the shear stress. Of exception is the surface heat transfer for CNTNf, which shows anti-enhancement behaviour, principally due to the interaction of the convective effects of the strongly viscous dominated momentum problem. More accurate representations of nanofluid thermophysical properties as functions of the volume fraction and fluid temperature are suggested. Specifically, additional experimental measurements of the properties of CNTNf and GNPNf and associated heat transfer and shear stress over a broad range of particle loadings are desired.

References

1. S.U.S. Choi, J.A. Eastman, *Enhancing thermal conductivity of fluids with nanoparticles*, in: ASME International Mechanical Engineering Congress & Exposition, San Fransisco, 1995.
2. S.K. Das, S.U.S. Choi, H.E. Patel, *Heat transfer in nanofluids – a review*, Heat Transfer Engineering, **27**, 10, 3–19, 2006. http://doi:10.1080/01457630600904593.
3. S.M.S. Murshed, C.A.N. de Castro (Eds.), *Nanofluids: synthesis, properties, and applications*, Nova Science Publishers, New York, 2014.
4. S.M.S. Murshed, C.A.N. de Castro, *Nanofluids as advanced coolants*, in: *Green Solvents I*, Springer, Netherlands, pp. 397–415, 2012 http://doi.org/10.1007/978-94-007-1712-1_14.
5. J. Buongiorno, *Convective transport in nanofluids*, Journal of Heat Transfer, **128**, 3, 240–250, 2006. http://doi.org/10.1115/1.2150834.
6. J.T.C. Liu, *On the anomalous laminar heat transfer intensification in developing region of nanofluid flow in channels or tubes*, Proceedings of the Royal Society A: Mathematical, Physical and Engineering Sciences, **468**, 2144, 2383–2398, 2012, http://doi.org/10.1098/rspa.2011.0671.
7. V. Trisaksri, S. Wongwises, *Critical review of heat transfer characteristics of nanofluids*, Renewable and Sustainable Energy Reviews, **11**, 3, 512–523, 2007, http://doi.org/10.1016/j.rser.2005.01.010.
8. M. Corcione, *Empirical correlating equations for predicting the effective thermal conductivity and dynamic viscosity of nanofluids*, Energy Conversion and Management, **52**, 1, 789–793, 2011. http://doi.org/10.1016/j.enconman.2010.06.072.
9. S.S. Murshed, C.N. de Castro, M. Lourenço, M. Lopes, F. Santos, *A review of boiling and convective heat transfer with nanofluids*, Renewable and Sustainable Energy Reviews, **15**, 5, 2342–2354, 2011, http://doi.org/10.1016/j.rser.2011.02.016.
10. K.V. Wong, O.D. Leon, *Applications of nanofluids: Current and future*, Advances in Mechanical Engineering, **2**, 519659, 2010, http://doi.org/10.1155/2010/519659.

11. J.T.C. LIU, M.E. FULLER, K.L. WU, A. CZULAK, A.G. KITHES, C.J. FELTEN, *Nanofluid flow and heat transfer in boundary layers at small nanoparticle volume fraction: Zero nanoparticle flux at solid wall*, Archives of Mechanics, **69**, 75–100, 2017, http://am.ippt.pan.pl/am/article/view/v69p75.

12. C.J. BARBOSA DE CASTILHO, M.E. FULLER, A. SANE, J.T.C. LIU, *Nanofluid flow and heat transfer in boundary layers at small nanoparticle volume fraction: Non-zero nanoparticle flux at solid wall*, Heat Transfer Engineering, **40**, (9–10), 725–737, 2019, http://doi.org/10.1080/01457632.2018.1442298.

13. D. HOPPER, D. JAGANATHAN, J.L. ORR, J. SHI, F. SIMESKI, M. YIN, J.T.C. LIU, *Heat transfer in nanofluid boundary layer near adiabatic wall*, Journal of Nanofluids, **7**, 6, 1297–1302, 2018, http://doi.org/10.1166/jon.2018.1551.

14. Y. LI, S. SUZUKI, T. INAGAKI, N. YAMAUCHI, *Carbon-nanotube nanofluid thermophysical properties and heat transfer by natural convection*, Journal of Physics: Conference Series **557**, 012051, 2014, http://doi.org/10.1088/1742-6596/557/1/012051.

15. J. MEYER, T. MCKRELL, K. GROTE, *The influence of multi-walled carbon nanotubes on single-phase heat transfer and pressure drop characteristics in the transitional flow regime of smooth tubes*, International Journal of Heat and Mass Transfer, **58**, 1-2, 597–609, 2013, http://doi.org/10.1016/j.ijheatmasstransfer.2012.11.074.

16. A. AMROLLAHI, A. RASHIDI, R. LOTFI, M.E. MEIBODI, K. KASHEFI, *Convection heat transfer of functionalized MWNT in aqueous fluids in laminar and turbulent flow at the entrance region*, International Communications in Heat and Mass Transfer, **37**, 6, 717–723, 2010, http://doi.org/10.1016/j.icheatmasstransfer.2010.03.003.

17. Y. DING, H. ALIAS, D. WEN, R.A. WILLIAMS, *Heat transfer of aqueous suspensions of carbon nanotubes (CNT nanofluids)*, International Journal of Heat and Mass Transfer, **49**, 1-2, 240–250, 2006, http://doi.org/10.1016/j.ijheatmasstransfer.2005.07.009.

18. P. GARG, J.L. ALVARADO, C. MARSH, T.A. CARLSON, D.A. KESSLER, K. ANNAMALAI, *An experimental study on the effect of ultrasonication on viscosity and heat transfer performance of multi-wall carbon nanotube-based aqueous nanofluids*, International Journal of Heat and Mass Transfer, **52**, 21-22, 5090–5101, 2009, http://doi.org/10.1016/j.ijheatmasstransfer.2009.04.029.

19. S. KAKAÇ, A. PRAMUANJAROENKIJ, *Review of convective heat transfer enhancement with nanofluids*, International Journal of Heat and Mass Transfer, **52**, 13-14, 3187–3196, 2009, http://doi.org/10.1016/j.ijheatmasstransfer.2009.02.006.

20. G.H. KO, K. HEO, K. LEE, D.S. KIM, C. KIM, Y. SOHN, M. CHOI, *An experimental study on the pressure drop of nanofluids containing carbon nanotubes in a horizontal tube*, International Journal of Heat and Mass Transfer, **50**, 23-24, 4749–4753, 2007, http://doi.org/10.1016/j.ijheatmasstransfer.2007.03.029.

21. Z.-H. LIU, L. LIAO, *Forced convective flow and heat transfer characteristics of aqueous drag-reducing fluid with carbon nanotubes added*, International Journal of Thermal Sciences, **49**, 12, 2331–2338, 2010, http://doi.org/10.1016 /j.ijthermalsci.2010.08.001.

22. H. XIE, H. LEE, W. YOUN, M. CHOI, *Nanofluids containing multiwalled carbon nanotubes and their enhanced thermal conductivities*, Journal of Applied Physics, **94**, 8, 4967, 2003, https://doi.org/10.1063/1.1613374.

23. W. Yu, H. Xie, X. Wang, X. Wang, *Significant thermal conductivity enhancement for nanofluids containing graphene nanosheets*, Physics Letters A, **375**, 10, 1323–1328, 2011, https://doi.org/10.1016/j.physleta.2011.01.040.

24. S.S. Sanukrishna, M.J. Prakash, *Exploiting the potentials of graphene nano-platelets for the development of energy-efficient lubricants for refrigeration systems*, in: Springer Transactions in Civil and Environmental Engineering, Springer, Singapore, pp. 303–312, 2002, https://doi.org/10.1007/978-981-15-1063-2_24.

25. A.S. Dalkiliç, H. Mercan, G. Özçelik, S. Wongwises, *Optimization of the finned double-pipe heat exchanger using nanofluids as working fluids*, Journal of Thermal Analysis and Calorimetry, https://doi.org/10.1007/s10973-020-09290-x.

26. J.P. Vallejo, U. Calviño, I. Freire, J. Fernández-Seara, L. Lugo, *Convective heat transfer in pipe flow for glycolated water-based carbon nanofluids. A thorough analysis*, Journal of Molecular Liquids, **301**, 112370, 2020, https://doi.org/10.1016/j.molliq.2019.112370.

27. A.O. Borode, N.A. Ahmed, P.A. Olubambi, *A review of heat transfer application of carbon-based nanofluid in heat exchangers*, Nano-Structures & Nano-Objects, **20**, 100394, 2019, https://doi.org/10.1016/j.nanoso.2019.100394.

28. S.S. Sanukrishna, A.V. Raju, A. Krishnan, G.H. Harikrishnan, A. Amal, T.S.K. Kumar, M.J. Prakash, *Enhancing the thermophysical properties of PAG lubricant using graphene nano-sheets*, Journal of Physics: Conference Series, **1355**, 012041, 2019, https://doi.org/10.1088/1742-6596/1355/1/012041.

29. A. Akbari, E. Mohammadian, S.A.A. Fazel, M. Shanbedi, M. Bahreini, M. Heidari, G. Ahmadi, *Comparison between nucleate pool boiling heat transfer of graphene nanoplatelet- and carbon nanotube- based aqueous nanofluids*, ACS Omega, **4**, 21, 19183–19192, 2019, https://doi.org/10.1021/acsomega.9b02474.

30. A.O. Borode, N.A. Ahmed, P.A. Olubambi, *Application of carbon-based nanofluids in heat exchangers: Current trends*, Journal of Physics: Conference Series, **1378**, 032061, 2019, doi.org/10.1088/1742-6596/1378/3/032061.

31. A.A. Hussien, M.Z. Abdullah, N.M. Yusop, W. Al-Kouz, E. Mahmoudi, M. Mehrali, *Heat transfer and entropy generation abilities of MWCNTs/GNPs hybrid nanofluids in microtubes*, Entropy, **21**, 5, 480, 2019, https://doi.org/10.3390/e21050480.

32. S. Hamze, N. Berrada, A. Desforges, B. Vigolo, T. Maré, D. Cabaleiro, P. Estellé, *Dynamic viscosity of purified MWCNT water and water-propylene glycol based nanofluids*, in: 1st International Conference on Nanofluids (ICNf2019), 2nd European Symposium on Nanofluids (ESNf2019), pp. 329–332, 2019.

33. D. Shi, Z. Guo, N. Bedford, *Carbon nanotubes*, in: *Nanomaterials and Devices*, Elsevier, pp. 49–82, 2015, https://doi.org/10.1016/b978-1-4557-7754-9.00003-2.

34. V. Harik, *Classification of carbon nanotubes*, in: *Mechanics of Carbon Nanotubes*, Elsevier, pp. 73–105, 2018, https://doi.org/10.1016/b978-0-12-811071-3.00004-4.

35. D.E.S. de Sousa, C.H. Scuracchio, G.M. de Oliveira Barra, A. de Almeida Lucas, *Expanded graphite as a multifunctional filler for polymer nanocomposites*, in: *Multifunctionality of Polymer Composites*, Elsevier, pp. 245–261, 2015, https://doi.org/10.1016/b978-0-323-26434-1.00007-6.

36. N. AHAMMED, L.G. ASIRVATHAM, S. WONGWISES, *Effect of volume concentration and temperature on viscosity and surface tension of graphene–water nanofluid for heat transfer applications*, Journal of Thermal Analysis and Calorimetry, **123**, 2, 1399–1409, 2016, https://doi.org/10.1007/s10973-015-5034-x.

37. D. WEN, Y. DING, *Experimental investigation into convective heat transfer of nanofluids at the entrance region under laminar flow conditions*, International Journal of Heat and Mass Transfer, **47**, 24, 5181–5188, 2004, https://doi.org/10.1016/ j.ijheatmasstransfer.2004.07.012.

38. H. BLASIUS, *Grenzschichten in Flüssigkeiten mit kleiner Reibung*, Zeitschrift für angewandte Mathematik und Physik, **56**, 1–37, 1908.

39. E. POHLHAUSEN, *Der Wärmeaustausch zwischen festen Körpern und Flüssigkeiten mit kleiner Reibung und kleiner Wärmeleitung*, ZAMM – Zeitschrift für angewandte Mathematik und Mechanik, **1**, 2, 115–121, 1921, https://doi.org/10.1002/zamm.19210010205.

40. M. XING, J. YU, R. WANG, *Experimental study on the thermal conductivity enhancement of water based nanofluids using different types of carbon nanotubes*, International Journal of Heat and Mass Transfer, **88**, 609–616, 2015, https://doi.org /10.1016/j.ijheatmasstransfer.2015.05.005.

41. L. CHEN, H. XIE, Y. LI, W. YU, *Nanofluids containing carbon nanotubes treated by mechanochemical reaction*, Thermochimica Acta, **477**, 1-2, 21–24, 2008, https://doi.org /10.1016/j.tca.2008.08.001.

42. T.X. PHUOC, M. MASSOUDI, R.-H. CHEN, *Viscosity and thermal conductivity of nanofluids containing multi-walled carbon nanotubes stabilized by chitosan*, International Journal of Thermal Sciences, **50**, 1, 12–18, 2011, https://doi.org/10.1016 /j.ijthermalsci.2010.09.008.

43. L. CHEN, H. XIE, W. YU, Y. LI, *Rheological behaviors of nanofluids containing multi-walled carbon nanotube*, Journal of Dispersion Science and Technology, **32**, 4, 550–554, 2011, https://doi.org/10.1080/01932691003757223.

44. M. MEHRALI, E. SADEGHINEZHAD, S. LATIBARI, S. KAZI, M. MEHRALI, M.N.B.M. ZUBIR, H.S. METSELAAR, *Investigation of thermal conductivity and rheological properties of nanofluids containing graphene nanoplatelets*, Nanoscale Research Letters, **9**, 1, 15, 2014, https://doi.org/10.1186/1556-276x-9-15.

45. C. SELVAM, D.M. LAL, S. HARISH, *Enhanced heat transfer performance of an automobile radiator with graphene based suspensions*, Applied Thermal Engineering, **123**, 50–60, 2017, https://doi.org/10.1016/j.applthermaleng.2017.05.076.

46. S. ASKARI, R. LOTFI, A. SEIFKORDI, A. RASHIDI, H. KOOLIVAND, *A novel approach for energy and water conservation in wet cooling towers by using MWNTs and nanoporous graphene nanofluids*, Energy Conversion and Management, **109**, 10–18, 2016, https://doi.org/10.1016/j.enconman.2015.11.053.

47. Z. SAID, R. SAIDUR, M. SABIHA, N. RAHIM, M. ANISUR, *Thermophysical properties of single wall carbon nanotubes and its effect on exergy efficiency of a flat plate solar collector*, Solar Energy, **115**, 757–769, 2015, https://doi.org/10.1016/j.solener.2015.02.037.

48. S. DINARVAND, *Nodal/saddle stagnation-point boundary layer flow of CuO–Ag/water hybrid nanofluid: a novel hybridity model*, Microsystem Technologies, **25**, 7, 2609–2623, 2019, https://doi.org/10.1007/s00542-019-04332-3.

49. A. Kuznetsov, D. Nield, *Natural convective boundary-layer flow of a nanofluid past a vertical plate*, International Journal of Thermal Sciences, **49**, 2, 243–247, 2010, https://doi.org/10.1016/j.ijthermalsci.2009.07.015.

50. M. Sheremet, I. Pop, *Conjugate natural convection in a square porous cavity filled by a nanofluid using Buongiorno's mathematical model*, International Journal of Heat and Mass Transfer, **79**, 137–145, 2014, https://doi.org/10.1016/j.ijheatmasstransfer.2014.07.092.

51. T. Muhammad, A. Alsaedi, S. A. Shehzad, T. Hayat, *A revised model for Darcy–Forchheimer flow of Maxwell nanofluid subject to convective boundary condition*, Chinese Journal of Physics, **55**, 3, 963–976, 2017, https://doi.org/10.1016/j.cjph.2017.03.006.

52. T. Hayat, T. Muhammad, S. Shehzad, A. Alsaedi, *On three-dimensional boundary layer flow of Sisko nanofluid with magnetic field effects*, Advanced Powder Technology, **27**, 2, 504–512, 2016, https://doi.org/10.1016/j.apt.2016.02.002.

53. M. Sheikholeslami, H.B. Rokni, *Numerical modeling of nanofluid natural convection in a semi annulus in existence of Lorentz force*, Computer Methods in Applied Mechanics and Engineering, **317**, 419–430, 2017, https://doi.org/10.1016/j.cma.2016.12.028.

54. M. Sheikholeslami, S. Shehzad, Z. Li, A. Shafee, *Numerical modeling for alumina nanofluid magnetohydrodynamic convective heat transfer in a permeable medium using Darcy law*, International Journal of Heat and Mass Transfer, **127**, 614–622, 2018, https://doi.org/10.1016/j.ijheatmasstransfer.2018.07.013.

55. A. Kuznetsov, D. Nield, *The Cheng–Minkowycz problem for natural convective boundary layer flow in a porous medium saturated by a nanofluid: A revised model*, International Journal of Heat and Mass Transfer, **65**, 682–685, 2013, https://doi.org/10.1016/j.ijheatmasstransfer.2013.06.054.

56. M. A. Sheremet, T. Grosan, I. Pop, *Free convection in a square cavity filled with a porous medium saturated by nanofluid using Tiwari and Das' nanofluid model*, Transport in Porous Media, **106**, 3, 595–610, 2014, https://doi.org/10.1007/s11242-014-0415-3.

57. A. Kuznetsov, D. Nield, *Natural convective boundary-layer flow of a nanofluid past a vertical plate: A revised model*, International Journal of Thermal Sciences, **77**, 126–129, 2014, https://doi.org/10.1016/j.ijthermalsci.2013.10.007.

58. T. Muhammad, A. Alsaedi, T. Hayat, S.A. Shehzad, *A revised model for Darcy–Forchheimer three-dimensional flow of nanofluid subject to convective boundary condition*, Results in Physics, **7**, 2791–2797, 2017, https://doi.org/10.1016/j.rinp.2017.07.052.

59. J. Buongiorno, D.C. Venerus, N. Prabhat, T. McKrell, J. Townsend, R. Christianson, Y.V. Tolmachev, P. Keblinski, L. Wen Hu, J.L. Alvarado, I. C. Bang, S.W. Bishnoi, M. Bonetti, F. Botz, A. Cecere, Y. Chang, G. Chen, H. Chen, S.J. Chung, M.K. Chyu, S.K. Das, R.D. Paola, Y. Ding, F. Dubois, G. Dzido, J. Eapen, W. Escher, D. Funfschilling, Q. Galand, J. Gao, P.E. Gharagozloo, K.E. Goodson, J.G. Gutierrez, H. Hong, M. Horton, K.S. Hwang, C.S. Iorio, S.P. Jang, A.B. Jarzebski, Y. Jiang, L. Jin, S. Kabelac, A. Kamath, M.A. Kedzierski, L.G. Kieng, C. Kim, J.-H. Kim, S. Kim, S.H. Lee, K.C. Leong, I. Manna, B. Michel, R. Ni, H. E. Patel, J. Philip, D. Poulikakos, C. Reynaud, R. Savino, P.K. Singh, P. Song, T. Sundararajan, E. Timofeeva, T. Tritcak, A.N. Turanov, S.V. Vaerenbergh, D. Wen, S. Witharana, C.Yang, W.-H. Yeh, X.-Z. Zhao, S.-Q. Zhou, *A benchmark study on the thermal conductivity of nanofluids*, Journal of Applied Physics, **106**, 9, 094312, 2009, https://doi.org/10.1063/1.3245330.

60. H. SCHLICHTING, *Boundary-Layer Theory*, 6th ed., McGraw-Hill, New York, 1968.

61. A. FICK, *Ueber diffusion*, Annalen der Physik und Chemie, **170**, 1, 59–86, 1855, https://doi.org/10.1002/andp.18551700105.

62. M.J. ASSAEL, I.N. METAXA, J. ARVANITIDIS, D. CHRISTOFILOS, C. LIOUTAS, *Thermal conductivity enhancement in aqueous suspensions of carbon multi-walled and double-walled nanotubes in the presence of two different dispersants*, International Journal of Thermophysics, **26**, 3, 647–664, 2005, https://doi.org/10.1007/s10765-005-5569-3.

63. A.C. HINDMARSH, *Scientific Computing*, North-Holland Publishing Company, 1983, Ch. ODEPACK, A Systematized Collection of ODE Solvers, pp. 55–64.

64. S.H. JOHN W. EATON, D. BATEMAN, R. WEHBRING, http://www.gnu.org/software /octave /doc/interpreter, version 4.0.0 manual: a high-level interactive language for numerical computations, 2015, http://www.gnu.org/software/octave/doc/interpreter.

65. J.C. MAXWELL, *A Treatise on Electricity and Magnetism*, Vol. 2, Clarendon Press, Oxford, 1881.

66. R. PRASHER, D. SONG, J. WANG, P. PHELAN, *Measurements of nanofluid viscosity and its implications for thermal applications*, Applied Physics Letters, **89**, 13, 133108, 2006, https://doi.org/10.1063/1.2356113.

Received April 29, 2020; revised version June 16, 2020.
Published online August 10, 2020.